nature communications

Article

https://doi.org/10.1038/s41467-025-59842-8

Lipids modulate the dynamics of GPCR:β-arrestin interaction

Received: 26 April 2024

Accepted: 5 May 2025

Published online: 29 May 2025

Check for updates

Antoniel A. S. Gomes[1,2,4], Michela Di Michele[1,4], Rita Ann Roessner[1], Marjorie Damian[1], Paulo M. Bisch[2], Nathalie Sibille[3], Maxime Louet[1], Jean-Louis Banères[1] & Nicolas Floquet[1]

β-arrestins are key molecular partners of G Protein-Coupled Receptors (GPCRs), triggering not only their desensitization but also intracellular signaling. Existing structural data point to high conformational plasticity of GPCR:β-arrestin interaction, with two completely different orientations between receptor and β-arrestin. Combining molecular dynamics simulations and fluorescence spectroscopy, we show that β-arrestin 1 interacts with membranes even in the absence of a receptor, an interaction that is enhanced by PI(4,5)P2, presumably holding the β-arrestin 1 C-edge loop into the lipid bilayer. This key interaction helps β-arrestin 1 to adopt a "receptor-ready" orientation and consequently favors its coupling to the ghrelin receptor (GHSR). In addition, we show that the GHSR:β-arrestin 1 assembly is a dynamic complex where β-arrestin can adopt several orientations. PI(4,5)P2 decreases the dynamics of the complex and shifts the equilibrium between the different arrangements, favoring one of them. Taken together, our results highlight how PI(4,5)P2 plays a true third-player role in the GPCR:β-arrestin interaction, not only by preparing β-arrestin for its further interaction with receptors but also by modulating its orientation once the protein:protein complex is formed.

GPCRs form a large family of over 800 transmembrane receptors whose activities are linked to a wide range of physiological functions. As such, they constitute privileged targets for the design of new drugs[1]. Their activities result from their coupling to intracellular effectors including G proteins, GPCR kinases (GRKs) and arrestins that all initiate different signaling responses[2]. In addition to GPCR desensitization, receptor-bound arrestins also initiate important signaling cascades, thus regulating a wide range of cellular functions[3]. Therefore, a better understanding of GPCR:β-arrestin interactions at the molecular scale is a key step for the design of novel drugs with biased signaling effects[4]. Mammals express four different arrestins; while arrestin-1 (rod) and arrestin-4 (cone) are visual arrestins that bind exclusively to light-activated phosphorylated rhodopsin, arrestin-2 (also called β-arrestin 1) and arrestin-3 (β-arrestin 2) are more ubiquitously expressed, regulating hundreds of different receptors[5]. This already indicates a high degree of adaptability for β-arrestins that can thus recognize a large number of different receptors despite their significantly different spatial distribution of amino acids and cellular environment. Available structures show that β-arrestins consist of two N- and C-terminal lobes flanking a central region called the "finger loop" that inserts directly into the intracellular transmembrane (TM) bundle of GPCRs (Fig. 1A). The N-domain lobe of β-arrestin is dedicated to the binding of phosphorylated residues[6,7] usually located in the C-tail or the intracellular loop-3 of receptors, again with a high degree of adaptability[8]. The C-terminal domain plays a direct role in the interaction of β-arrestin with membranes; this interaction involves (1) a plausible insertion of its "C-edge loop" into the lipid bilayer[9], and (2) the binding of phosphatidylinositol-4,5-bisphosphates (PI(4,5)P2)[10]

[1]Institut des Biomolécules Max Mousseron (IBMM), UMR 5247 CNRS, Université de Montpellier, ENSCM, Montpellier cedex 5, France. [2]Laboratório de Física Biológica, Instituto de Biofísica Carlos Chagas Filho, Universidade Federal do, Rio de Janeiro, Brazil. [3]Centre de Biologie Structurale (CBS), CNRS, Université de Montpellier, Inserm, Montpellier, France. [4]These authors contributed equally: Antoniel A. S. Gomes, Michela Di Michele.
e-mail: nicolas.floquet@umontpellier.fr

https://doi.org/10.1038/s41467-025-59842-8

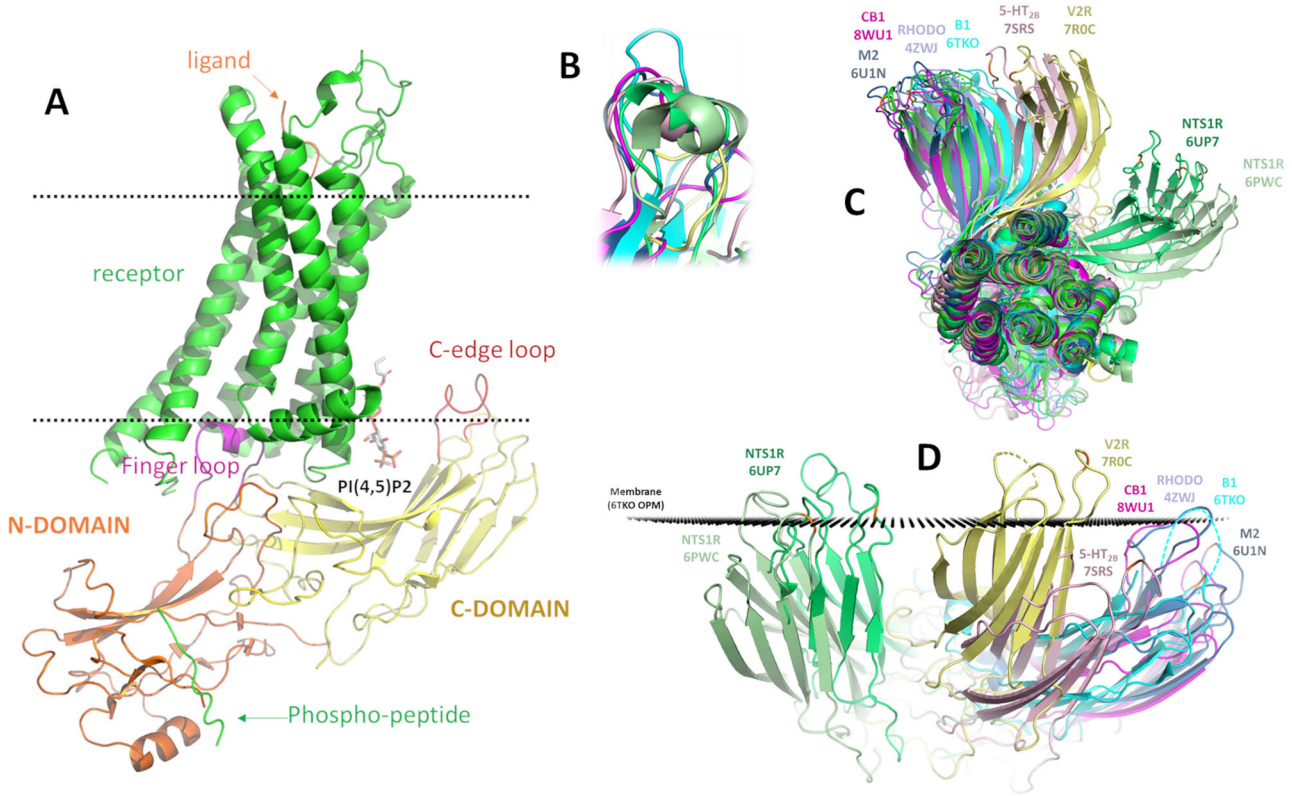

Fig. 1 | Conformational plasticity of the GPCR:β-arrestin interaction in existing structural data. A Summary of β-arrestin contacts with the receptor and with the membrane as observed in the NTS1R structure (PDB: 6UP7). **B** Conformations adopted by the finger-loop of β-arrestin in the different receptors. **C** Orientations of β-arrestin in the different known structures of GPCR:β-arrestin complexes showing two main sets of orientations with NTS1R structures aside. **D** Position of the C-edge loop of β-arrestin with respect to the membrane among the same set of structures; black points correspond to the position of the membrane predicted by OPM (Orientations of Proteins in Membrane)[58] for the complex with the beta-1 adrenergic receptor (B1AR) (PDB: 6TKO).

and its derivatives[11,12] to a specific site. Most of the available structures in the Protein Data Bank (PDB) describe β-arrestin complexed to different GPCRs in a "core-engaged" mode. In all these structures, the finger loop of β-arrestin is inserted into the TM helix bundle of the receptor, displaying an intriguing wide diversity of conformations different from those observed in isolated β-arrestins (Fig. 1B), whereas this loop represents the main point of contact with the receptors. Core-engaged structures include those with rhodopsin (PDBs: 4ZWJ[13], 5DGY[14], and 5W0P[15]), beta-1 adrenergic (B1AR, PDB: 6TKO[16]), neurotensin-1 (NTS1R, PDBs: 6PWC[17] and 6UP7[10]), M2 muscarinic (PDB: 6U1N[18]), vasopressin 2 (V2R, PDB: 7R0C[19]), serotonin 5-HT_{2B} (PDB: 7SRS[20]) and cannabinoid 1 (CB1, PDB: 8WU1)[21] receptors. Two other recent structures have also shown that β-arrestin can bind to the glucagon receptor (GCGR, PDB: 8JRU and 8JRV)[22] without this engagement of the finger loop, in a so-called "tail-engaged" mode. Although limited, this set of structures already sheds light on the high degree of plasticity of GPCR:β-arrestin interactions. In the core-engaged structures, the overall orientation of β-arrestin in the protein:protein complex indeed shows a quasi-rigid body rotation around 75° in the two NTS1R structures with respect to the M2, B1AR, visual rhodopsin and CB1 structures (Fig. 1C). In this respect, the Vasopressin 2 and 5-HT_{2B} receptor structures can be considered as intermediate orientations. Another key point of this plasticity concerns the putative insertion of the C-edge loop of β-arrestin in the membrane (Fig. 1D), as suggested in some structures (mainly those describing PI(4,5)P2 bound to the C-domain). However, since most of these structures were obtained in detergents rather than in a lipid bilayer, it remains difficult to assess whether this loop is effectively inserted into the membrane under more physiological conditions. Until now, these structural differences were mainly attributed to the nature of the coupled receptor and have been proposed to possibly help β-arrestin adapt to the different phosphorylation schemes of GPCRs[23].

Here we leverage molecular dynamics (MD) simulations and site-directed fluorescence spectroscopy with an isolated receptor in lipid nanodiscs to characterize the interaction of β-arrestin 1 with membranes in the absence or presence of the ghrelin receptor (GHSR), a prototypical class-A GPCR involved in growth hormone secretion, food intake[24] and metabolic homeostasis[25]. By doing so, we reveal structural features on the dynamics of the GPCR:β-arrestin arrangement and the impact of the membrane environment on these dynamics.

Results

PI(4,5)P2 increases β-arrestin:membrane interactions

To analyze the ability of the human β-arrestin 1 to interact with membranes, a fluorescent probe, monobromobimane (MB), was first inserted at positions 68 or 191 of a cysteine-free mutant of wild-type β-arrestin 1 (mutated cysteines are reported in the methods section). This cysteine-free mutant will be referred to as wild-type β-arrestin 1 throughout the text. The first modification (position 68, shown in orange in Fig. 2A) has been extensively used in the field to probe GPCR:β-arrestin interactions, as changes in MB emission report on the insertion of the finger loop of β-arrestin in the receptor core[26–28]. The second modification, with the probe at position 191 of β-arrestin 1 (Fig. 2A, reported in green) was designed to monitor the insertion of the C-edge loop in the lipid bilayer. Labeling of this same residue with a ^{19}F probe was recently used to monitor insertion of β-arrestin 1 into the lipid bilayer of nanodiscs[29]. We then analyzed the emission properties of MB-labeled β-arrestin 1 in the absence or presence of POPC/POPG nanodiscs with or without 2.5% PI(4,5)P2, a ratio we

https://doi.org/10.1038/s41467-025-59842-8

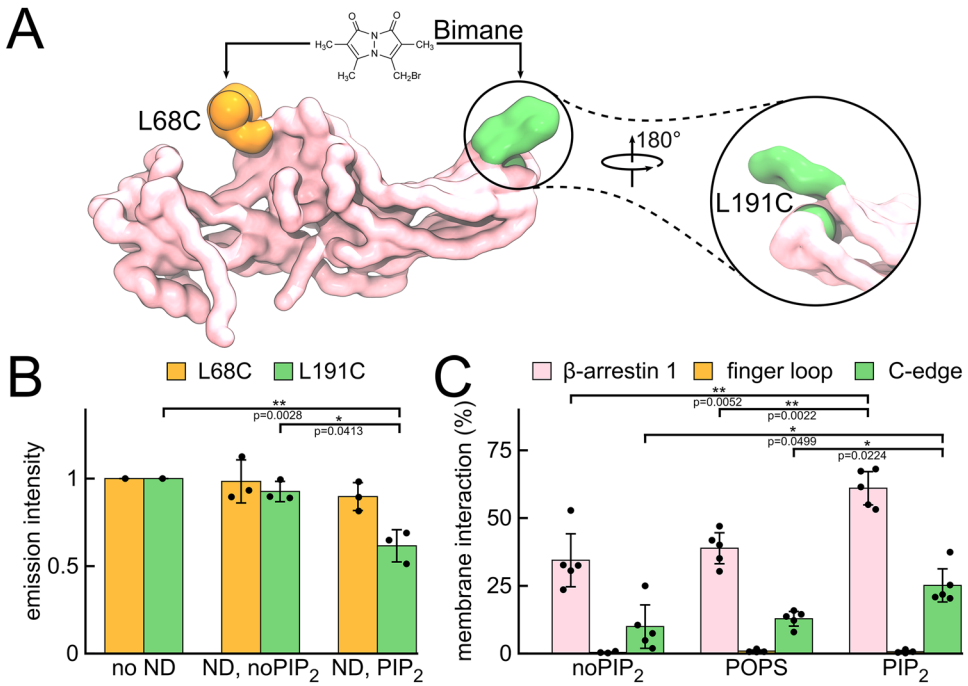

Fig. 2 | Structural aspects of β-arrestin 1 and its interaction with membranes. **A** Side view of the β-arrestin 1 model used CGMD simulations. The protein backbone beads are shown as pink surface representations with the finger loop and the C-edge loop highlighted in orange and green, respectively. Residues chosen to insert MB are depicted as orange (L68C) and green spheres (L191C). **B** Changes in the MB normalized emission intensity for the two positions of wild-type β-arrestin 1 labeling in the absence of nanodiscs (no ND), in the presence of POPC/POPG nanodiscs (ND, no PIP2), or in the presence of POPC/POPG nanodiscs containing 2.5% PI(4,5)P2 (ND, PIP2). Data were inferred from the emission spectra (see Supplementary Fig. 2) and are the mean value ± SD of three experiments. **C** Percentages of CGMD simulation frames where β-arrestin 1, the finger loop, or the C-edge loop are in contact with the membrane are shown as a function of the simulated system (β-arrestin 1 in the presence of a PI(4,5)P2-free, PI(4,5)P2-enriched, or POPS-enriched membrane). Bars correspond to the means and standard deviations calculated over five independent simulations. All statistical values in (**B**) and (**C**) were determined using one-way ANOVA tests with Bonferroni correction between all groups (*$p \le 0.05$, **$p \le 0.01$).

showed to be required for a maximal effect on GHSR function[30]. In addition, spin-labeled phosphatidylcholine (PC) was included into the nanodiscs to trigger significant changes in MB emission upon insertion of the probe into the bilayer in the absence of receptor (see experimental procedures in Methods, and emission spectra in Supplementary Fig. 1). Adding this labeled lipid into the nanodiscs was required in particular for position 191. Indeed, a change was observed for the probe at this position in POPC/POPG-only nanodiscs (Supplementary Fig. 2), likely reflecting the positioning of the probe in a more apolar environment. However, this change was of low amplitude, so that the presence of spin-labeled PC in the nanodisc was necessary to unambiguously report on MB proximity to the lipid bilayer. Such a limited change in the absence of the fluorescence quencher may indicate that the MB probe was not inserted deeply into the bilayer when attached at position 191.

In both the absence and presence of PI(4,5)P2 in the nanodiscs, no change in the MB emission was observed when the probe was located in the finger loop of β-arrestin 1. This suggests that this region remained distant from the membrane surface independently of the composition of the lipid nanodisc (Fig. 2B). With respect to the probe at position 191, no change was observed with POPC/POPG-only nanodiscs, suggesting that, under such conditions, the C-edge loop centered around residue 191 remained distant from the quencher-containing lipid for a major fraction of labeled β-arrestin. The absence of any effect of the quenching group was not likely due to a deep insertion of MB into the bilayer while the spin label was on the lipid headgroup. Indeed, no effect was observed either when the quenching moiety was located on the acyl chain of a lipid (5-doxyl-stearic acid; Supplementary Fig. 3). Besides, in the absence of its labeling with MB, we cannot exclude that the other C-edge loop centered around residue 340 of β-arrestin 1 inserts into the membrane in the absence of PI(4,5)P2 whereas that around residue 191 would not. It should be noted, however, that in the case of rhodopsin, quenching of emission was observed for bimane attached to both positions, suggesting a simultaneous insertion of the two loops[9]. Such a concomitant insertion was also reported for β-arrestin 2 where both loops were predicted to anchor the protein into the lipid bilayer[31].

In contrast to what was observed in the absence of PI(4,5)P2, a change in the emission properties of MB attached to C191 of β-arrestin 1 was observed when the nanodiscs contained 2.5% PI(4,5)P2 (Fig. 2B). Essentially, only the emission intensity was affected, with a less pronounced effect on the maximum wavelength (see spectra in Supplementary Fig. 1). This may again reflect that the probe was not deeply inserted in the lipid bilayer under such conditions and that most of the effect on MB emission was related to the proximity of MB to the quenching group in the headgroup of the labeled lipid. Altogether, this suggests that this region of β-arrestin 1 comes in close proximity to the lipid bilayer of the nanodiscs, but essentially when these include PI(4,5)P2.

We finally verified that the behavior of β-arrestin 1 observed here was not affected by its activation state. To this end, we duplicated the MB fluorescence experiments with a variant of β-arrestin 1 lacking its C-terminal region (β-arrestin 1 (1-382)), which has been proposed to be in a pre-activated state[32]. This truncated β-arrestin 1 protein was previously used in the cryo-EM structures of the complexes with several GPCRs[10,18,19]. In addition, this also allowed a direct comparison with the data obtained with this same truncated β-arrestin 1 in the presence of

unphosphorylated GHSR in the discs (see below). As in the case of the wild-type protein, a cysteine-free mutant of the truncated β-arrestin 1 was used to allow its site-specific labeling. This variant will be referred to as ΔC β-arrestin 1 throughout the text. A larger change in MB emission was observed with ΔC β-arrestin 1 labeled on its C-edge loop and nanodiscs containing PI(4,5)P2 compared to the wild-type protein, suggesting a slight increase in the population of the protein being close to the membrane under such conditions (Supplementary Fig. 4). This is consistent with recent observations that the linewidth of ^{19}F probes in the C-edge loops is affected in the ΔC variant, suggesting that this modification may facilitate the C-edge-membrane interaction[29]. This could be indicative of an interplay between PI(4,5)P2 binding, membrane interaction and β-arrestin activation, as recently proposed[29,33,34].

To complement the fluorescence measurements, which remain limited in terms of structural resolution, and get a molecular picture of this β-arrestin:membrane interaction, we then performed coarse-grained molecular dynamics (CGMD) simulations starting with β-arrestin 1 located at a minimal distance above 20 Å from the bilayer (*i.e.* a distance higher than the cutoff distance which was set to 11 Å) to prevent any initial bias. 5 simulations of 30 μs were performed using the MARTINI 3 Force Field[35] and a membrane composition related to that of the lipid nanodiscs, replacing or not 10 POPC lipids by PI(4,5)P2 in each leaflet aiming to capture the specific effect of this lipid (this corresponds to a proportion of PI(4,5)P2 of 3%, close to the 2.5% used in the fluorescence experiments). The major difference with the experiments was that in the latter no cholesterol was added to the nanodiscs, as the concomitant addition of this molecule and PI(4,5)P2 made difficult to strictly control the lipid composition of the discs. This is consistent with recent data demonstrating that disparities in lipid incorporation in nanodiscs occur upon the addition of compounds that affect the rigidity of the membrane and/or when using complex lipid compositions[36]. The simulations first confirmed the ability of the C-edge loop of β-arrestin 1 to spontaneously insert into the lipid bilayer during 25.1 ± 6.4% and 9.9 ± 8.0% of the time with and without PI(4,5)P2, respectively (Fig. 2C).

In contrast, position 68 was barely in contact with the membrane (0.7 ± 0.4% and 0.4 ± 0.2% of the time with and without PI(4,5)P2, respectively) (Fig. 2C), thus confirming the experimental results and indicating a preferred β-arrestin orientation at the membrane surface. In contrast to the experiments, however, our simulations predicted a notable proportion of β-arrestin 1 at the membrane surface, even in the absence of PI(4,5)P2 (61 ± 6.1% and 34.4 ± 9.8% of the time with and without PI(4,5)P2, respectively) (Fig. 2C). This overestimation could plausibly be explained by the finite size of the simulation box that considerably increases the probability of interaction of the protein with the membrane, although unbinding events of β-arrestin 1 to the membrane occurred during the simulations both with and without PI(4,5)P2 (Supplementary Fig. 5). Accordingly, we can reasonably anticipate that the interaction of the C-edge loop with the membrane would contribute to increasing these differences on longer time scales as those corresponding to the experiments. Due to their positioning in space (Supplementary Fig. 6A), we can note that a quasi-identical behavior with respect to the membrane was observed for the two arrestin C-edge loops, *i.e.* that containing the residue 191 used in our study for the insertion of the probe and that containing the residue 340 used as a reference in previous studies (Supplementary Fig. 6B).

We also investigated the effect of phosphatidylserine (POPS), a negatively charged phospholipid, in β-arrestin 1 binding to the membrane. We found that POPS does not affect the interaction of β-arrestin 1 with the membrane, showing similar results as those without PI(4,5)P2 (Fig. 2C and Supplementary Fig. 5). This confirmed that the observed effect is indeed PI(4,5)P2-specific and not only due to the negatively charged headgroups of lipids.

Supporting the experiments, our computational results suggest a particular orientation of β-arrestin 1 at the membrane surface corresponding to an insertion of the C-edge loop into the bilayer and a position more distant from the surface for the finger loop (Fig. 3A). This orientation is consistent with the presence of PI(4,5)P2 in the previously identified cleft located in the C-domain of β-arrestin 1[10]. To better understand how PI(4,5)P2 could contribute to the binding of β-arrestin 1 to the membrane and to this specific orientation, we computed the spatial occupancy of the PI(4,5)P2 headgroups on the β-arrestin surface along all CGMD trajectories and at different thresholds (0.3, 0.5 and 0.7% of the total frames). Although these thresholds are low (less than 1% of total frames), the percentages of frames reported consider all β-arrestin 1 orientations explored in our CGMD simulations, including unbound and bound to the membrane surface. Interestingly, we retrieved an interaction hotspot for PI(4,5)P2 that exactly matches the region of the C-domain previously identified (Fig. 3B). This region is enriched with positively charged residues, such as K250 and K324, previously identified as important binders for phosphatidylinositols[10]. This emphasizes the ability of the MARTINI force field to successfully predict PI(4,5)P2 binding at protein surfaces, as we already recently reported for the isolated GHSR[30].

Distributions of the "tilt" and "roll" angles (Fig. 3C and methods for a detailed procedure) of β-arrestin 1 during our CGMD simulations (Fig. 3D) clearly showed the same preferred orientation at the membrane surface of β-arrestin 1 independently of the presence of PI(4,5)P2 and corresponding to restrained "tilt" values around 5-35° and "roll" values largely distributed in the range 40-140°. The same analysis performed on POPC and POPS not only confirmed that β-arrestin 1 displayed "tilt" and "roll" angles at the membrane surface but also that PI(4,5)P2 could contribute to maintaining the protein closer to the membrane surface, as previously observed in Fig. 2. Two subsets of orientations could indeed be defined from the obtained distributions corresponding to a "tilt" value of about 20° and to "roll" values of either 60° or 120°. The increased interaction of β-arrestin 1 with the membrane in the presence of PI(4,5)P2 contributed to enriching the populations of both sub-states with a slight preference for the one corresponding to the lower "roll" value (Fig. 3D). "Tilt" and "roll" angles were calculated from existing structures of GPCR:β-arrestin complexes deposited in the PDB, after receptor alignment to B1AR (PDB: 6TKO)[16], interestingly yielded values within the preferred distribution regions from our CGMD simulations (Fig. 3D). Analysis of the full distribution (Supplementary Fig. 7A) of "tilt" and "roll" angles throughout the trajectories helped to characterize other orientations of β-arrestin 1 at the membrane surface (Supplementary Fig. 7B, C). In these orientations, the PI(4,5)P2 interacted at the bottom of the C-edge loop (Supplementary Fig. 7B) and with the N-domain of β-arrestin 1 (Supplementary Fig. 7C), indicating secondary, less specific sites for PI(4,5)P2. The first site comprises residues K229 and R331, possibly contributing to the retention of the C-edge loop in the bilayer after its anchoring. In the second site, we identified K11 and R25 as essential for stabilizing PI(4,5)P2. These two secondary binding sites are known for recognizing inositides[37] whereas the N-domain secondary binding site also plays a role in recognizing GPCR phosphorylated C-terminal residues before receptor desensitization[6,15].

Together, our results indicate that isolated β-arrestin 1 presumably adopts an orientation at the membrane surface directly compatible with the interaction with GPCRs, with PI(4,5)P2 further contributing to increasing the frequency of this orientation by stabilizing the position of the C-edge loop in the bilayer.

PI(4,5)P2 favors the interaction of β-arrestin 1 with GHSR

To further explore the role of PI(4,5)P2 in the β-arrestin:membrane:receptor interplay, the MB emission experiments were repeated in the presence of agonist-activated GHSR in the lipid nanodiscs. First, we used the ΔC β-arrestin 1 variant. This C-terminus

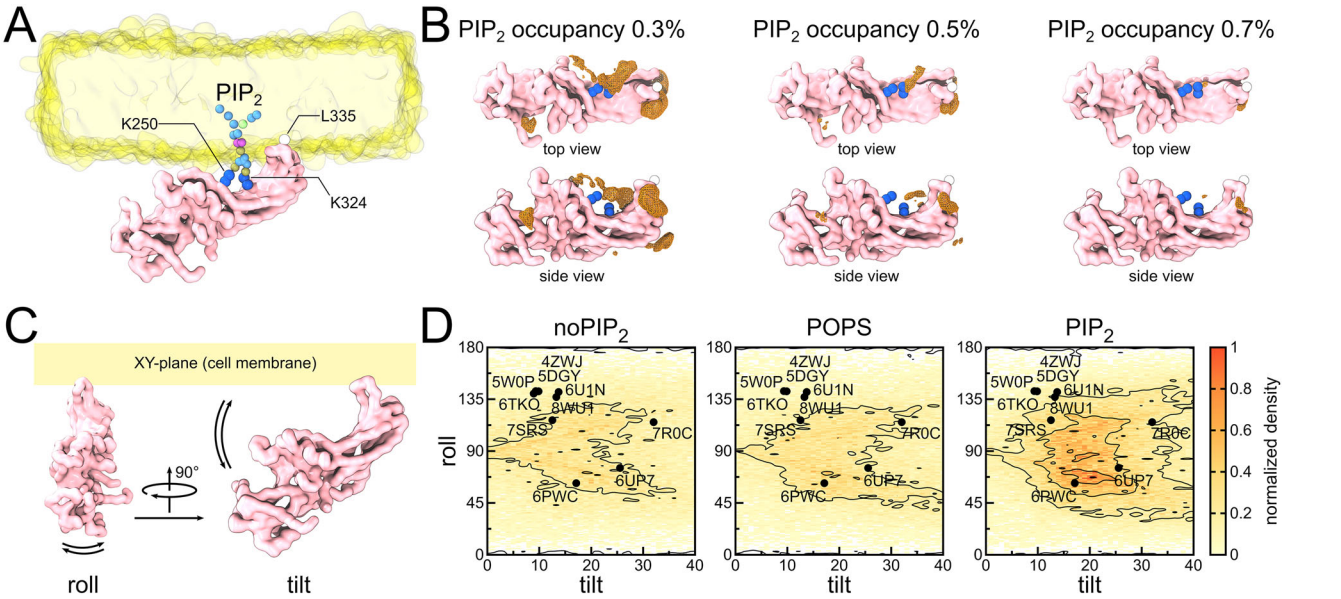

Fig. 3 | β-arrestin 1 interaction with PI(4,5)P2 and predicted orientations to the cell membrane. A PI(4,5)P2 binding site encompassing positively charged residues (K250 and K324) and the membrane insertion of C-edge through a hydrophobic residue (L335) are shown. **B** Statistical distributions of PI(4,5)P2 (orange meshes) along the obtained CGMD trajectories. It confirmed the specific binding of PI(4,5)P2 in the same site as that described in the literature[30]. Secondary sites distributed around the C-edge loop and the N-domain of β-arrestin 1 were also found. **C** The definition of "tilt" and "roll" angles aimed to report the position of the protein with respect to the membrane surface. **D** β-arrestin 1 assumes a specific orientation at the membrane surface (see line contours), compatible with further interaction with receptors. Black dots correspond to "tilt" and "roll" angles extrapolated from existing GPCR:β-arrestin structures in the PDB after receptor alignment to B1AR (PDB: 6TKO).

truncated arrestin mutant has been shown to bind agonist-activated GPCRs regardless of their phosphorylation status[32]. Hence, it circumvents the requirement for receptor phosphorylation, as in our case GHSR was expressed in a prokaryotic system and could not thus be directly phosphorylated in the expressing cells. As shown in Fig. 4A, a change in the emission properties of MB attached to the ΔC β-arrestin 1 finger loop (C68) was observed with nanodiscs containing MK0677-activated unphosphorylated GHSR, whether PI(4,5)P2 was present or not in the nanodiscs, consistent with our previous reports[24]. These changes affected both the maximum emission wavelength (blue shift) and intensity (Supplementary Fig. 1), indicative of a possible alteration of the physico-chemical properties of the probe environment upon insertion of the finger loop into the receptor core[38]. Since the changes in C68-MB emission do not distinguish between receptor and nanodisc engagement, we could not strictly exclude at this stage that they were caused by the proximity of the finger loop to the lipid bilayer in a tail-only configuration of the GHSR:β-arrestin 1 complex. However, in this case, a decrease in the emission intensity should have been observed because of the presence of the quenching group in the bilayer. In contrast to C68, the emission properties of MB attached to C191 changed only when PI(4,5)P2 was present, similarly to receptor-free nanodiscs. To be noted, as in the case of empty nanodiscs, the changes in the maximum emission wavelength for MB attached to C191 were of limited amplitude (Supplementary Fig. 1). This suggests that, even in the presence of the receptor, the probe is not deeply inserted in the bilayer, in contrast to what was reported with visual arrestin and rhodopsin for a closely related position[9]. Altogether, our observations suggest a possible model in which pre-activated β-arrestin 1 could interact with the receptor core independently of its interaction with the lipid bilayer, with a concomitant membrane proximity of the C-edge loop occurring only in the presence of PI(4,5)P2.

To assess whether this membrane insertion could favor the interaction of β-arrestin 1 with GHSR, we repeated the experiment with wild-type β-arrestin 1 and unphosphorylated GHSR. As shown in Fig. 4B and Supplementary Fig. 1, a slight change in the emission properties of MB attached to C68 was observed, but only when the lipid nanodiscs contained PI(4,5)P2, *i.e.* under conditions where the C-edge loop inserts into the bilayer. This suggests a possible model where interaction of the C-edge loop of β-arrestin 1 into the lipid bilayer, favored by the presence of PI(4,5)P2, could overcome, at least to a slight, limited extent, the requirement of β-arrestin 1 activation by the receptor phosphorylated C-terminal region[34].

PI(4,5)P2 promotes B1AR orientation of β-arrestin in the complex with GHSR

Currently, it is not clear whether the insertion of β-arrestin 1 C-edge loop in the bilayer caused by the presence of PI(4,5)P2 could impact the dynamics of the complex with the receptor. Until recently, only the shifted structures of the NTS1R receptor were indeed captured in the presence of PI(4,5)P2[10] mimetics. However, the recently solved structures for the vasopressin 2[19] and serotonin 5-HT_{2B}[20] receptors demonstrated that other (intermediate) orientations of β-arrestin are also compatible with the lipid bound to the same pocket. To address this key question, we built two homology models of the GHSR:β-arrestin 1 complex using the two extreme orientations observed with the NTS1R (PDB: 6UP7)[10] and B1AR (PDB: 6TKO)[16] as templates (Fig. 5). Using these two models, we then selected several positions to insert fluorescent probes that would allow us to explore experimentally the orientation of β-arrestin 1 with respect to GHSR. Namely, we selected $F71^{1.60}$ for GHSR, as this residue had already been mutated to a single reactive cysteine and subsequently labeled with fluorescent probes in a previous analysis of the interaction of the isolated receptor in nanodiscs and G proteins[39]. For β-arrestin 1, we selected residues 167 and 191, as they should report on the position of the receptor with respect to β-arrestin's N- and C-domains. Moreover, these positions had already been modified for β-arrestin 1 intramolecular FRET experiments, and showed to do not affect the functional properties of this protein with regard to its interaction with GHSR in nanodiscs[23]. Although the $71^{1.60}$:167 distance poorly discriminates the different orientations of β-arrestin in the receptor:β-arrestin complex (Fig. 5), as

https://doi.org/10.1038/s41467-025-59842-8

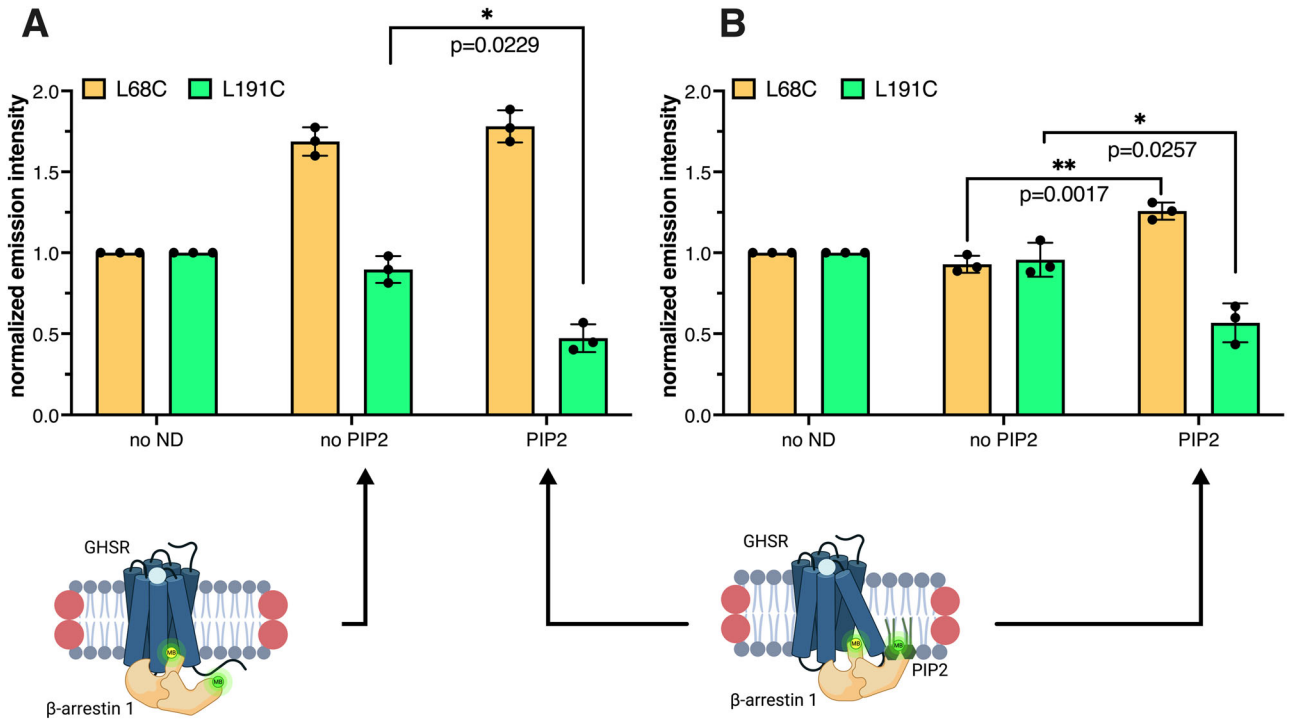

Fig. 4 | Role of the PI(4,5)P2 in the interaction of β-arrestin 1 with GHSR. **A** Changes in the emission intensity of MB attached to either C68 or C191 of ΔC β-arrestin 1 free in solution (no ND), in the presence of POPC/POPG nanodiscs containing unphosphorylated GHSR and 10 μM MK0677 (ND, no PIP2) or in the presence of POPC/POPG nanodiscs containing 2.5% PI(4,5)P2, unphosphorylated GHSR and 10 μM MK0677 (ND, PIP2). The scheme was created in BioRender. BANERES, J. (2025) https://BioRender.com/ ngj6am4. **B** Same experiment with wild-type β-arrestin 1 instead of ΔC β-arrestin 1. The scheme was created in BioRender. BANERES, J. (2025) https://BioRender.com/aha8piq. In all cases, data are the mean value ± SD of three experiments. Statistical values were obtained by means a one-way ANOVA test with Bonferroni post-test groups (*$p \le 0.05$, **$p \le 0.01$).

stated below, it nevertheless reports on the core engagement of β-arrestin 1 with GHSR, and as such allows to rule out any possible tail-only engaged complex (see Table 1). On the contrary, the $71^{1.60}$:191 distance was much more informative to distinguish the different orientations of β-arrestin in the complex, as it is significantly different in structures of β-arrestin 1 complexes :about 34 Å in the complex with NTS1R, in the 55–63 Å range for other core-engaged receptors and around 21 Å in the tail-engaged mode (see Table 1).

We then analyzed the interaction between MK0677-activated GHSR and β-arrestin 1 by monitoring the LRET signal between the receptor labeled with Alexa Fluor 488 or BodipyTMR at position $71^{1.60}$ and β-arrestin 1 labeled with a Tb cryptate donor either at position 167 or at position 191. For the $71^{1.60}$:167 pair, Alexa Fluor 488 was used as the fluorescence acceptor, as the R_0 value with the Tb cryptate as the donor, i.e. in the 39 Å range, is in the range of the expected distance values. For the $71^{1.60}$:191 pair, BodipyTMR was used as the acceptor as it displays a higher R_0 value (in the 51 Å range) compatible with distances in the 40–60 Å range. We used LRET, as this technique has several technical advantages over conventional FRET, including distance measurement with greater accuracy, and insensitivity to incomplete labeling[40]. To circumvent any possible bias due to the use of an unphosphorylated receptor and the pre-activated ΔC β-arrestin 1, we instead used here wild-type β-arrestin 1 and sortase to enzymatically ligate to the GHSR transmembrane core a synthetic peptide where the potential phosphorylation sites in the GHSR C-terminal domain[41] had been replaced by their phosphorylated counterpart (see experimental procedures in Methods). Of importance, the interaction pattern observed with this receptor variant and wild-type β-arrestin 1 was similar to that obtained with the wild-type GHSR phosphorylated in vitro with recombinant GRK5 (Supplementary Fig. 8). Although low amounts of purified protein were obtained using this ligation approach, this strategy ensured homogeneous phosphorylation of the receptor compared to in vitro phosphorylation with recombinant GRK, justifying its use in the present experiments. The LRET profiles were thus recorded with this modified GHSR inserted into nanodiscs with or without 2.5% PI(4,5)P2 (Fig. 6). In all cases, the profiles were fitted with a multi-exponential, with two major components, a slow and a fast one (Supplementary Table 1). For the $71^{1.60}$:167 pair, only a weak, almost non-significant difference was observed between the profiles obtained for nanodiscs with or without PI(4,5)P2, certainly because the distances are too close for this pair and not well adapted to discriminate different orientations (see above). This was not the case for the $71^{1.60}$:191 pair, where a significant difference was observed between both conditions, probably because of a larger difference for the distance between the probes in the different possible orientations (Table 1).

The distance between the LRET donor and acceptor was then approximated from the mean sensitized-emission lifetimes of these two components, and their relative populations approximated from the pre-exponential factors and the excited state lifetime values (see Supplementary Table 1)[42]. As shown in Fig. 6E, F, the emission decays corresponded to the distance between the probes in the same range, independently of the presence of PI(4,5)P2 in the nanodisc. These were in the same range as those estimated for the major orientations observed in the cryo-EM structures. The occurrence of different distances between the probes was indicative of a dynamic complex, where several orientations could co-exist in solution. However, the relative population of these arrangements was dependent on the presence of PI(4,5)P2 in the nanodiscs. Indeed, in the latter case, one of the orientations appeared to be favored. This suggests that insertion of the C-edge of β-arrestin 1 into the bilayer in the presence of PI(4,5)P2 in the nanodiscs was associated to a decrease in the dynamics of the complex this protein formed with the agonist-activated GHSR. It should be noted, however, that the fit of the LRET profiles was unlikely to discriminate species with closely related lifetimes and/or

https://doi.org/10.1038/s41467-025-59842-8

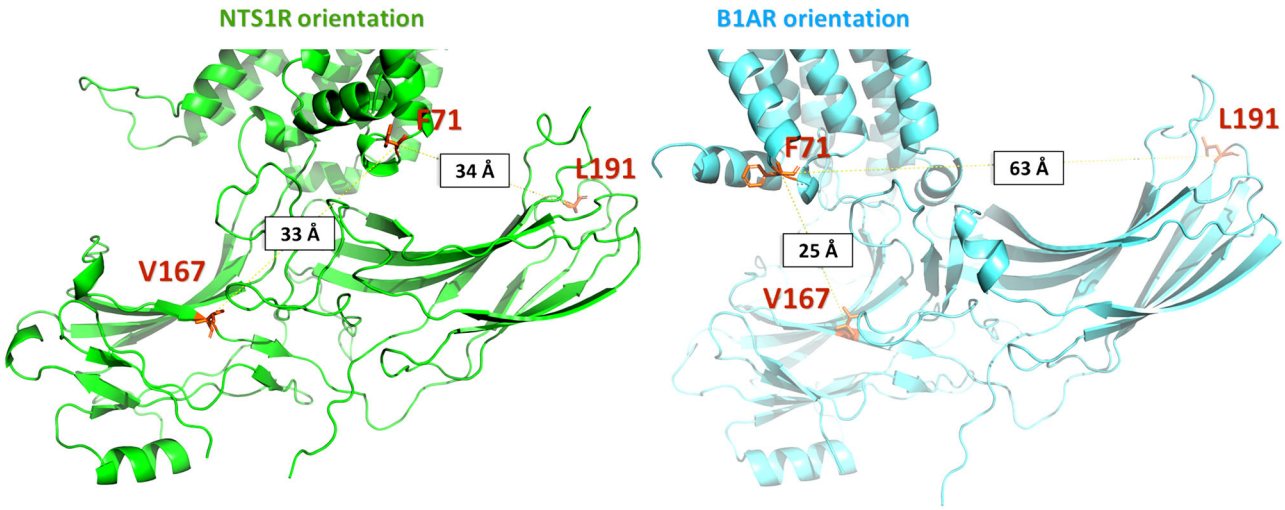

Fig. 5 | Distinct orientations of β-arrestin 1 coupled to the GHSR. Models of the GHSR:β-arrestin 1 complex built from NTS1R (green, PDB: 6UP7) or B1AR (blue, PDB: 6TKO) structures. The location of the residues used to attach the fluorescent probes in β-arrestin 1 (V167 or L191) and in GHSR ($F71^{1.60}$) are depicted in orange sticks.

populations, in particular given the mean error of the experimental data. Therefore, at this stage, we cannot exclude the occurrence of species with some different orientations or of differences in the population of the complexes. Taken together, these observations nevertheless suggest that the interaction of β-arrestin 1 with the lipid bilayer due to the presence of PI(4,5)P2 in the nanodisc decreases the dynamics of the complex this protein forms with the receptor, possibly favoring one arrangement of the complex or, alternatively, decreasing the exchange rate between the different positions.

To get a molecular view of how PI(4,5)P2 could contribute to promoting the B1AR-like orientation of β-arrestin 1 in the complex with GHSR, we performed CGMD simulations starting from the two extreme orientations already depicted in Fig. 5. A standard elastic network with some minor modifications was defined as classically done in studies in which the MARTINI force field is used. First, we suppressed the springs involving residues of the finger loop so that the latter could adapt to the receptor, as shown in the available structures (Fig. 1D). The same was done for residues of the intracellular loop 3 (ICL3) of the receptor, which is not seen in existing GHSR structures, indicative of its high flexibility. It must be noted that in both NTS1R-like and B1AR-like starting models, the C-edge loop of β-arrestin 1 was in a favorable position to be initially inserted in the lipid bilayer. Finally, a restraint was added to the finger loop to maintain it inside the receptor core during the simulations, thus limiting any release of β-arrestin 1 from the receptor's core. 20 simulations of 30 μs were obtained starting from both orientations in the presence or absence of PI(4,5)P2 (four different systems corresponding to a total simulation amount of 2.4 ms). To follow the orientation of β-arrestin 1 with respect to the receptor, we defined a rotation angle using the *x* and *y* components of the vector defined by residues $F71^{1.60}$ of the receptor and L191 of β-arrestin 1 (after alignment onto the receptor's backbone beads) and taking the NTS1R-like orientation as a reference (Fig. 7A). Thus, values around 0° indicate an NTS1R-like orientation whereas values around 75° correspond to a B1AR orientation. The distributions reported in Fig. 7B indicated no spontaneous transition from the B1AR-like to the NTS1R-like arrangement regardless of the presence of PI(4,5)P2. On the contrary, starting from the NTS1R-like orientation, several transitions towards the B1AR-like orientation were observed, which were decreased by the presence of PI(4,5)P2. These results suggest that the transition between the two orientations can be observed without the dissociation of the complex. The 2D plot of Fig. 7C computed from simulations starting from the NTS1R-like orientation interestingly showed a good correlation between the β-arrestin 1 rotation angle and the $F71^{1.60}$:L191 distance, with two main populations centered around 34 and 60 Å, respectively, in agreement with the values measured in the experiments.

Computing the probabilities of PI(4,5)P2 contacts around the complex showed significant differences between the B1AR-like and the NTS1R-like arrangement, possibly explaining the preference for the B1AR-like orientation in the presence of PI(4,5)P2 (Fig. 7D). First, an additional PI(4,5)P2 binding site was observed at the interface between TM6 and TM7, which was of particular interest as we already suggested that the binding of PI(4,5)P2 in this region contributes to maintaining an active conformation of the GHSR[30]. Second, an increased presence of PI(4,5)P2 was noted at the bottom of the C-edge loop in the same site previously observed for the isolated β-arrestin 1 (report to Fig. 3B and Supplementary Fig. 7B for comparison). Taken together, our results suggest that PI(4,5)P2 stabilizes the B1AR-like orientation via specific interactions with both protein partners.

To confirm this possibility of a different distribution of PI(4,5)P2 around the complex according to the orientation of β-arrestin 1, we performed all-atom simulations starting from the same models with three different replicas for each system (B1AR/NTS1R, PIP2/no PIP2), each lasting 2 μs. No transition between the two orientations was observed in the related trajectories (Supplementary Fig. 9A). Nevertheless, we observed a distribution of PI(4,5)P2 around the complex closely related to that captured in our CGMD simulations, including the sites 1, 2, and 3 described for the isolated receptor and the additional site at the bottom of the C-edge loop of β-arrestin 1 (Supplementary Fig. 9B–D). As observed in our CGMD simulations, an increased presence of PI(4,5)P2 was captured in site 3 in the B1AR-like orientation.

C-edge loop release facilitates transitions between both conformations

To mechanistically study the influence of PI(4,5)P2 on the transition of the GHSR:β-arrestin 1 complex between the described conformations, we performed metadynamics simulations aiming to promote transitions in both directions (not only from NTS1R-like to B1AR-like as already observed in free CGMD, but also from B1AR-like to NTS1R-like). Due to its strong correlation with the β-arrestin 1 rotation angle, we used the F71:191 distance as a collective variable. We obtained 20 simulation replicas of ~15 μs long starting from both orientations in the presence or absence of PI(4,5)P2 (four systems corresponding to a total simulation time of 1.2 ms). Overall, the free energy profiles resulting from these CG metadynamics simulations revealed the

https://doi.org/10.1038/s41467-025-59842-8

Table. 1 | Intermolecular distances measured to discriminate between the different orientations of β-arrestin 1 in its receptor-bound state

Distance	NTS1R (PDB: 6PWC)	NTS1R (PDB: 6UP7)	V2R (PDB: 7ROC)	5-HT2B (PDB: 7SRS)	CB1 (PDB: 8WU1)	M2 (PDB: 6U1N)	RHODO (PDB: 4ZWJ)	B1AR (PDB: 6TKO)	GCGR (PDB: 8JRV)
71:167	34.4	33.1	32.1	34.8	34.3	33	28.9	25.6	45.5
71:191	34.8	34	55	57.6	59.7	62.6	62.5	63.1	21.5

Distances between residue $71^{1.60}$ of GHSR and either residues 167 or 191 of β-arrestin 1, as measured in all available GPCR:β-arrestin complexes in the PDB. All orientations correspond to the "core-engaged" form except the last one (GCGR = "tail-engaged") added for comparison.

existence of two equivalent minima compatible with the measured distances of the two orientations of β-arrestin 1 (Supplementary Fig. 10). In agreement with our unbiased MD simulations, CG metadynamics frequently captured transitions between both conformations, although transitions from B1AR-like to NTS1R-like were also captured to a lesser extent. Accordingly, and as done for the unbiased MD simulations, we selected only the CG metadynamics simulations that sampled a high number of transitions (*i.e.* starting from the NTS1R-like orientation) for further analysis. These simulations presented multiple back-and-forth transitions between the two orientations (Supplementary Fig. 11). Depending on the β-arrestin 1 rotation angle, the obtained snapshots were grouped into three subsets corresponding to NTS1R-like (0 ± 10°) and B1AR-like (70 ± 10°) conformations and those corresponding to transitions between both arrangements. Based on the different interaction profiles of the C-edge loop with PI(4,5)P2 depending on the conformation of GHSR:β-arrestin 1 complex (Fig. 7D), we calculated its position in the sampled trajectory subsets (Fig. 8).

The effect of PI(4,5)P2 to enhance the interaction of the C-edge loop with the membrane was detected to varying degrees in the different subgroups of conformations. While in B1AR-like snapshots the loop was on average always located at the membrane surface independent of the lipid composition (Fig. 8A, B), in NTS1R-like snapshots PI(4,5)P2 significantly increased the interactions between the C-edge loop and the membrane. Interestingly, even though the same tendency was observed in the sample of intermediate conformations governing the transition, here, the C-edge loop was always detached from the membrane (Fig. 8A, B). Our results suggest that the C-edge loop detaches from the membrane to facilitate the transitions between NTS1R and B1AR conformations. Consequently, the persistent anchoring of the C-edge loop in the B1AR conformation may explain why we did not observe spontaneous B1AR-to-NTS1R transitions in our unbiased CGMD simulations. Equally, these observations are in line with the reduced spontaneous transitions from NTS1R-like to B1AR-like in the presence of PI(4,5)P2 along our unbiased CGMD simulations. Taken together, we hypothesize that PI(4,5)P2 not only stabilizes the B1AR-like conformation as shown in LRET experiments and unbiased MD simulations but probably equally increases the energy barrier required for the transition from one conformation to the other.

Discussion

There is increasing evidence that the membrane environment influences the conformational dynamics and pharmacological properties of GPCRs. In this context, we have used computational and fluorescence approaches to provide evidence for a direct interaction of β-arrestin 1 with the membrane, which is modulated by a specific lipid moiety, PI(4,5)P2. In addition, we showed that the GHSR:β-arrestin 1 coupling is a dynamic process that may involve multiple assemblies. The membrane environment influenced the arrangement and dynamics of these assemblies, as the presence of PI(4,5)P2 significantly affected the relative distribution of the different states. Taken together, our results pave the way for a detailed understanding of the molecular processes underlying the allosteric modulation of GPCRs by PI(4,5)P2 and, by extension, other lipids.

We recently demonstrated that PI(4,5)P2 is involved in the activation of GHSR and its ability to further activate its G protein partner[30]. Here, we provide evidence that PI(4,5)P2 not only affects GHSR-catalyzed G protein activation but also β-arrestin 1 recruitment. Indeed, our data indicate that PI(4,5)P2 favors β-arrestin 1 coupling to GHSR inserted into lipid nanodiscs, in agreement with previous data reporting a similar effect, especially for GPCRs that transiently interact with β-arrestins[34], which is the case of GHSR. To be noted, nanodiscs have some limitations compared to other membrane-mimicking models, let alone cellular systems, that could explain some differences with previous reports on the interaction of β-arrestins with

https://doi.org/10.1038/s41467-025-59842-8

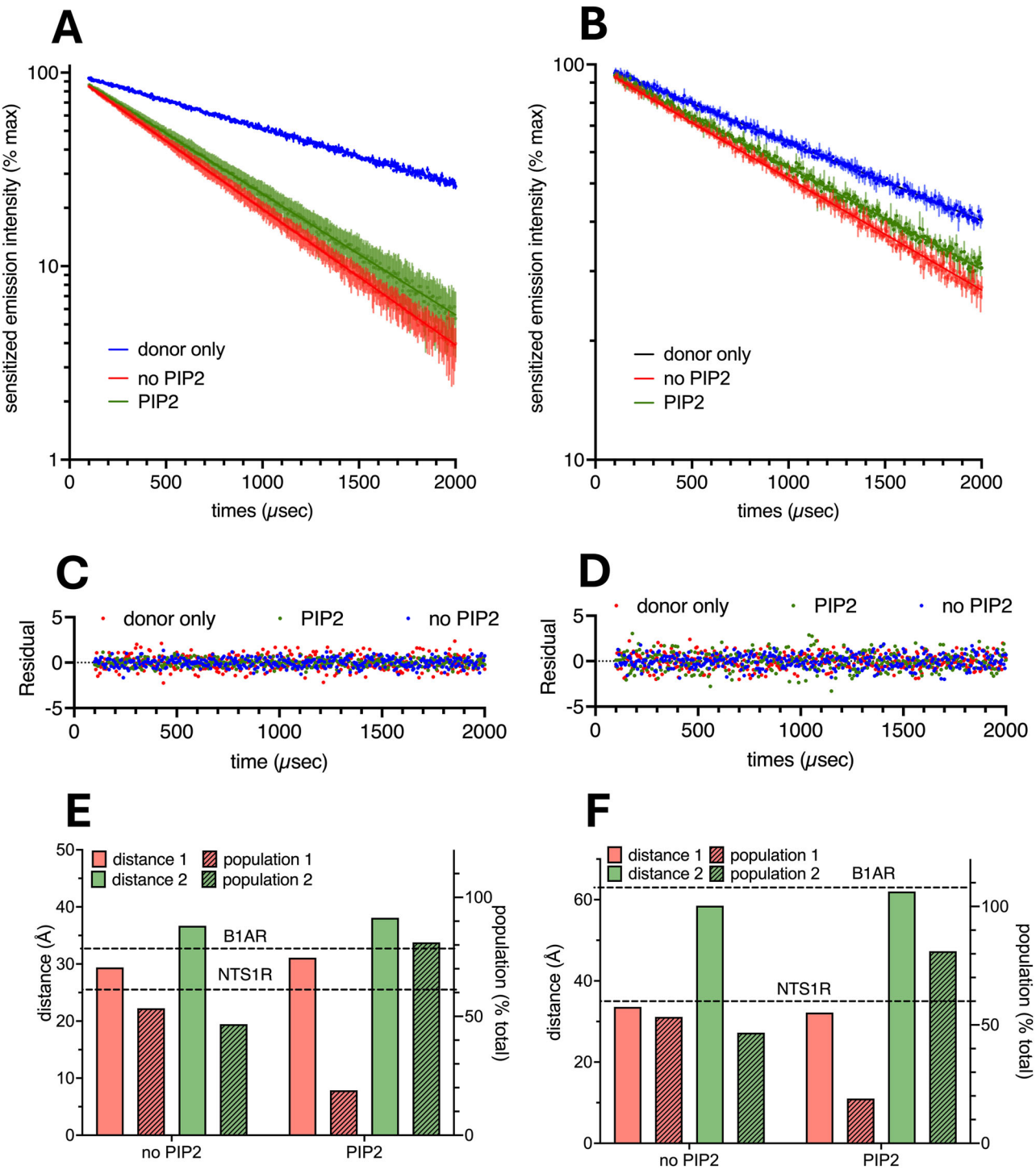

Fig. 6 | Relative orientation of the protein components in the GHSR:β-arrestin 1 complex. Sensitized-emission decays from phosphorylated GHSR labeled with Alexa Fluor 488 (**A**) or Bodipy-TMR (**B**) on C711.60 and assembled in nanodiscs containing or not 2.5% PI(4,5)P2, in the presence of wild-type β-arrestin 1 labeled either on C167 (**A**) or on C191 (**B**) with Lumi-4 Tb, and of 10 μM MK0677. Data are presented as the log of normalized fluorescence intensity as a function of time and are the mean ± SD of three independent measurements. (**C**, **D**) Corresponding residual values representing the goodness of the multi-exponential fits. (**E**, **F**) Corresponding mean distances and molecular fractions (populations) between the fluorescent probes calculated from the sensitized-emission lifetimes of the two dominant exponential components of the mean sensitized-emission decays (see Supplementary Table 1). The distances between the two probes calculated from the cryo-EM structures of the two representative orientations, *i.e.* NTS1R and B1AR (Table 1), are indicated in dotted lines.

membranes. For example, although the use of larger scaffolding proteins can help to overcome this problem, nanodiscs are still limited in the membrane surface available for protein-lipid interactions. They also have a limited ability to mimic some of the bulk properties of the lipid bilayer, such as lateral pressure or curvature. Finally, they still poorly mimic the complexity of the natural cell membranes in terms of lipid and protein diversity as well as bilayer asymmetry. Despite these limitations, nanodiscs have proven to be an invaluable tool for solution-state studies of integral membrane proteins in a lipidic environment. In particular, because they allow the insertion of the

https://doi.org/10.1038/s41467-025-59842-8

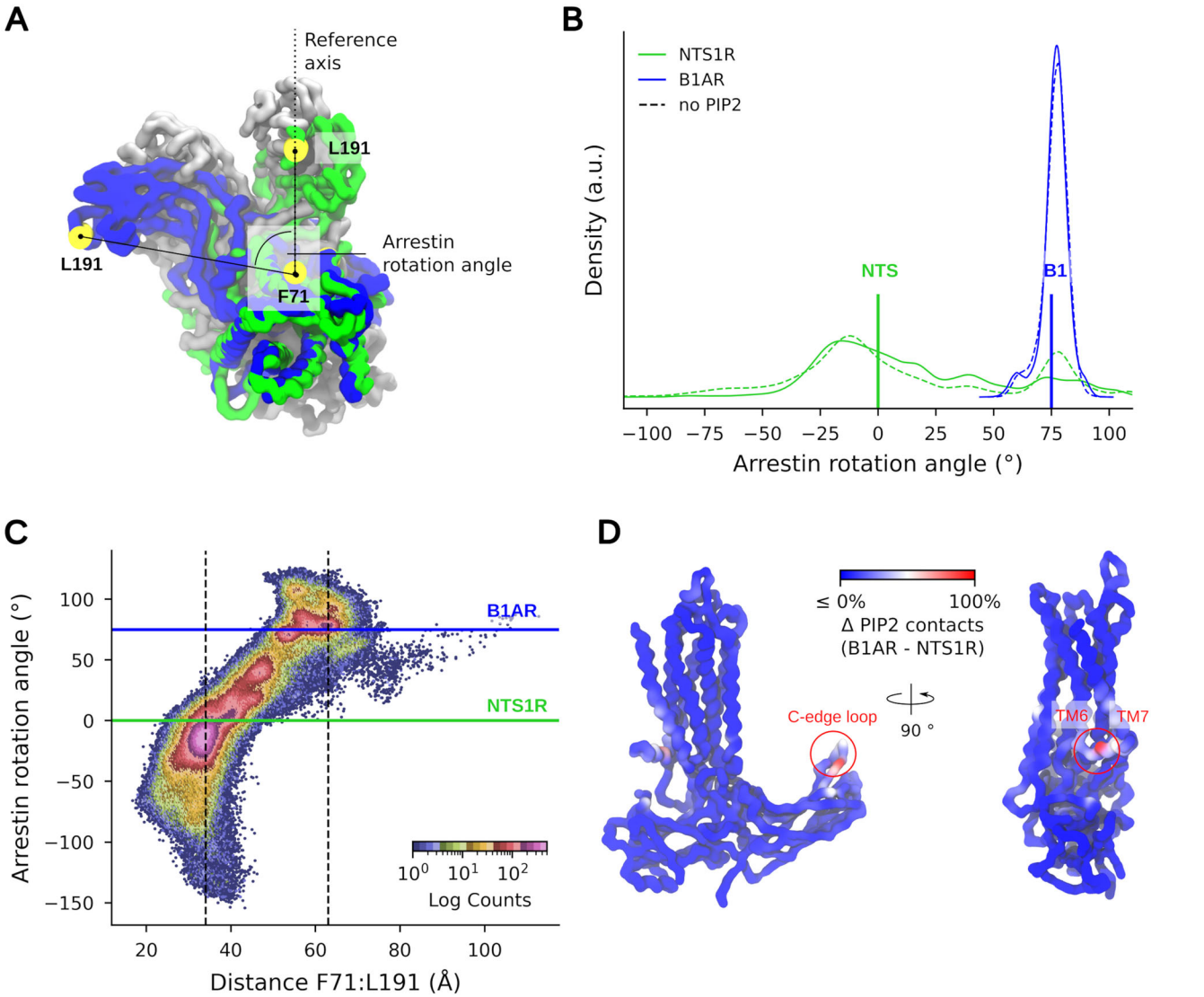

Fig. 7 | Results from CGMD simulations of the GHSR:β-arrestin 1 complex starting from the NTS1R-like or B1AR-like orientations. A Top views of snapshots from a CGMD simulation replica of the GHSR:β-arrestin 1 complex with the protein backbone beads being shown as surface representations. The NTS1R-like starting conformation is highlighted in green, intermediate conformations are shown in gray, and the fully B1AR-like transitioned complex is depicted in blue. The residues used for the rotation angle and the F71$^{1.60}$:L191 distance measurement are shown as yellow discs. **B** Distribution of the rotation angle of β-arrestin 1 for all CGMD simulation replicas starting from the NTS1R-like (green) and the B1AR-like orientation (blue) performed with (solid line) or without PI(4,5)P2 (dashed line). The rotation angles of the respective experimental structures are highlighted by vertical lines. **C** 2D histogram corresponding to data obtained starting from the NTS1R-like orientation and showing the correlation between the β-arrestin 1 rotation angle and the F71$^{1.60}$:L191 distance that was measured experimentally. The rotation angles of the NTS1R-like (green) and B1AR-like (blue) experimental structures are indicated by horizontal lines. **D** The difference in the percentage of frames where PI(4,5)P2 interacts with the protein complex between the simulation replica starting from the B1AR-like or the NTS1R-like orientation is mapped onto the backbone beads. Residues colored in red indicate a more frequent interaction of the respective beads with PI(4,5)P2 in simulations starting from the B1AR-like conformation whereas residues colored in blue show no differences between both conformations.

protein of interest into a bilayer while strictly controlling the lipid composition, they open the way to analyze the contribution of individual lipids to the receptor-effector coupling process, as illustrated here with PI(4,5)P2. As such, they represent a significant advance over other systems used to stabilize the fold of membrane proteins in biophysical analyses, particularly detergents.

Besides the recruitment to the agonist-activated receptor, we also observed a spontaneous, GHSR-independent interaction of β-arrestin 1 with the bilayer, which is modulated by PI(4,5)P2. This aligns with previous reports with β-arrestin 1 in more integrated cellular systems[31,43], suggesting that β-arrestin could operate at the membrane independently of its activating receptor[31]. To be noted, however, in the latter studies, binding of β-arrestin 2 to the plasma membrane involved the C-edge loops, as is the case here, but the PI(4,5)P2 binding site appeared dispensable. Whether the requirements for PI(4,5)P2 we observed here depend on the protein subtypes or result from the different membrane systems used (nanodiscs *vs* cells or supported bilayers) is an open question. Besides, whether in our system the interaction with the lipid bilayer affects the conformational equilibria of β-arrestin is also to be further assessed. Indeed, we did not investigate here the conformational state of this protein in the different conditions we explored (i.e. with or without proximity to the lipid bilayer). However, recent data indicated that PI(4,5)P2 induced partially activated β-arrestin 1 conformations[29], which could therefore be the case here.

The role of the β-arrestin's C-edge in the interactions with the membrane surface was first suggested through site-directed fluorescence measurements[44] and further confirmed through other

https://doi.org/10.1038/s41467-025-59842-8

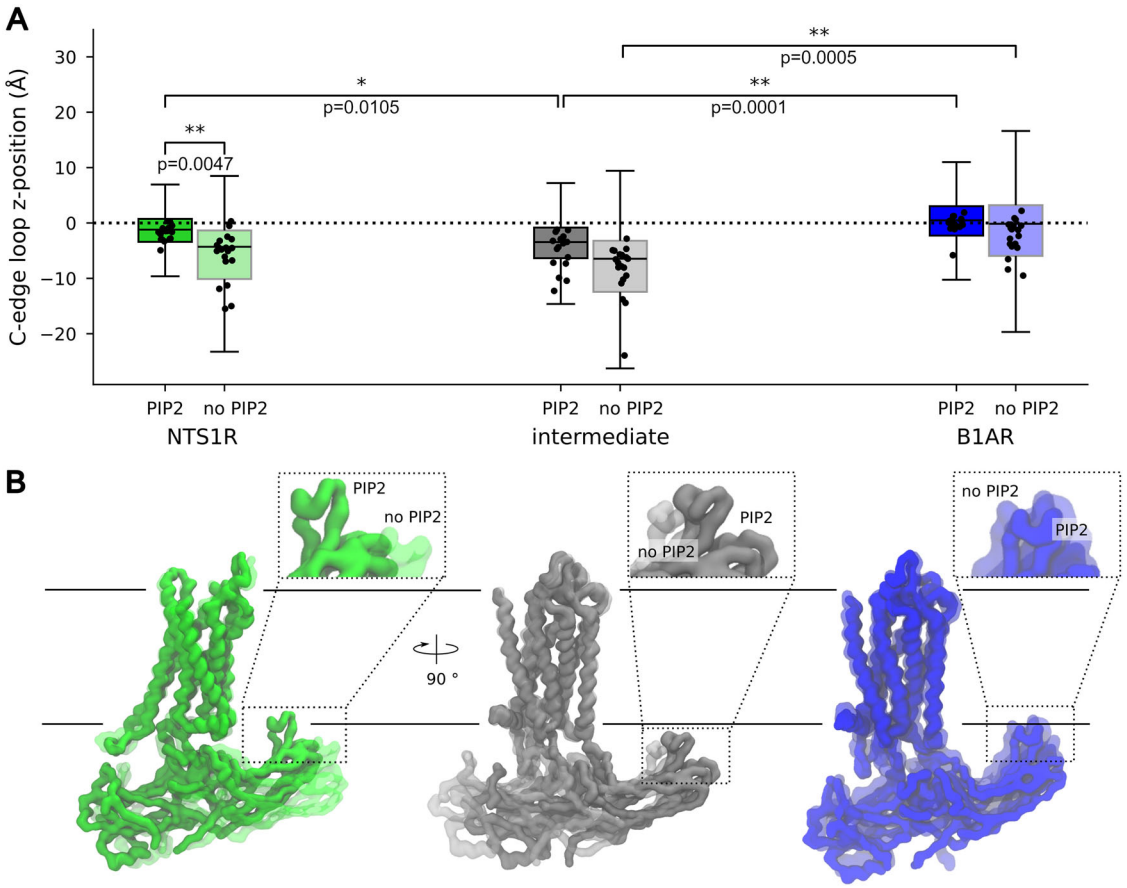

Fig. 8 | Influence of the C-edge loop-membrane interaction on the conformational equilibrium of the GHSR:β-arrestin 1 complex. A Boxplot showing the distribution of the C-edge loop z-position from NTS1R-like (green), B1AR-like (blue), and intermediate snapshots (gray) in the presence (dark) or absence of PI(4,5)P2 (light). Only CG metadynamics trajectories starting from the NTS1R-like orientation were considered in this analysis. The box represents the interquartile range (IQR), with the lower and upper hinges indicating the first (Q1) and third (Q3) quartiles, respectively. The line inside the box denotes the median. The whiskers extend to the smallest and largest values within 1.5 times the IQR from the hinges. The dotted line corresponds to the position of the intracellular membrane surface. Statistical values were determined using unpaired Student's t-tests with Bonferroni correction on the mean values of $n = 20$ independent simulation replicas, which are presented as black scatter ($^*p \le 0.05$, $^{**}p \le 0.01$). **B** Side views of representative snapshots from a CG metadynamics trajectory starting from the NTS1R orientation in the presence (dark) and absence of PI(4,5)P2 (light). The protein backbone beads are shown as surface representations with the same color scheme as in **A**. The intra- and extracellular membrane surfaces are depicted as black lines.

approaches[31]. Accordingly, our data point to the C-edge loop as a critical element in the β-arrestin 1:membrane interplay in all cases, *i.e.* in the absence or presence of the ghrelin receptor, also consistent with previous MD simulation reports[31,45]. Hence, this C-edge loop appears as a central element in β-arrestin coupling and activation, certainly cooperating with other structural elements (finger loop, phosphate sensor, polar core, etc.) to achieve signaling patterns. To be noted, the orientation adopted by β-arrestin 1 at the bilayer surface in the absence of GHSR was closely related to that it adopts in the different complexes with GPCRs reported to date. This suggests a model in which the interaction with the bilayer would prepare β-arrestin for its recruitment to the activated receptor. If this is the case, then its pre-association with the membrane would play a critical role in β-arrestin 1 function by facilitating its interaction with the receptor and subsequent activation. This would be consistent with recent single-molecule microscopy observations in which β-arrestin spontaneously pre-associates with the lipid bilayer, allowing it to diffuse laterally until it encounters activated receptors[31,43].

Several cryo-EM structures of GPCR:β-arrestin complexes have been solved so far. Notably, these structures report different orientations of β-arrestin relative to the receptor. One possibility would be that these different orientations depend on the conditions used to obtain these structures (sample engineering, receptor phosphorylation, complex preparation, detergents versus lipid bilayers, etc.). Alternatively, it has been proposed that these orientations are receptor-specific, in particular related to the presence of a phosphorylated ICL3 or a short C-tail on the GPCR[17]. The data we obtained here with GHSR indicate that this receptor makes a dynamic complex with β-arrestin 1 where several arrangements, including some close to the reported cryoEM structures, could coexist for the same receptor. This suggests that GPCR:β-arrestin coupling is a dynamic process, consistent with recent cross-linking experiments[46]. Importantly, the distribution of different states was here directly influenced by the nature of the lipid environment surrounding the receptor, namely the presence of PI(4,5)P2 molecules bound to specific sites. One possibility would therefore be that, for the same GPCR, different arrangements of the receptor:β-arrestin complex could occur. The stability of these states would depend on the environment, here the lipids, and possibly other features such as the phosphorylation status of the receptor (the so-called phospho-barcode[8]). Although we have no experimental and/or computational evidence at this stage of the analysis, it is tempting to then speculate that these different arrangements of the complex could be associated with (subtly) different conformational states of β-arrestin, with direct consequences for its functional properties.

Of note, our work does not take into account the impact of different phosphorylation patterns on the arrangement of the GHSR:β-

arrestin 1 complex. Increasing data point to the fact that GPCR phosphorylation motifs modulate arrestin interaction[47]. In our experimental setup, we used either a phosphorylation-independent β-arrestin 1 mutant or a receptor C-tail where all possible sites were phosphorylated. These included S362 and T366 that are primarily responsible for β-arrestin binding as well as S349 and T350 that play a role in the stability of the resulting complex[41]. The absence of any further detailed knowledge on the GRK-dependent phosphorylation barcode of GHSR, besides the full repertoire of possibly modified residues, prevented us from testing distinct patterns in the fluorescence assays. This is a limitation of our study. In the same manner, the impossibility of rationally constructing a complete, phosphorylated model of the GHSR is another limitation to comparing models and experiments. Indeed, the GHSR is phosphorylated on its C-terminal part[41], for which there is no template in the PDB (for any known receptor); without any structural information either on this part of the receptor nor in terms of its contacts with β-arrestin 1, it is uncertain to envisage the building of this C-terminus which is thought to be highly flexible. Moreover, as stated above, GHSR may be phosphorylated at different positions and several phosphorylation patterns may co-exist[41], making it even more difficult to choose one pattern in particular. Finally, the choice of an initial orientation of the C-terminal part of the receptor on the β-arrestin surface is not obvious, especially considering the multiple possible orientations of β-arrestin in the complex[10] and such a choice could completely condition the results of the simulations. In this context, we can actually not emphasize if a binding mode in which β-arrestin contacts the receptor core without being anchored to the membrane could exist with a phosphorylated receptor. Keeping this in mind, our MD simulation data presented in Figs. 7 and 8 were done to analyze the effect of PI(4,5)P2 in the context of the complex, even if no phosphorylation is present in our models. These calculations were carried out using a force that maintains the finger loop inside the receptor, thus forcing the coupled state to be stabilized.

Although our computational results indicate that the C-edge detachment from the membrane facilitates conformational transitions, determining if β-arrestin completely decouples the receptors during this process remains an open question and requires further experiments. Whatever the details, our data nevertheless indicate that GPCR:β-arrestin coupling is an inherently dynamic process under the control of multiple inputs, among them the membrane environment. As such, the latter appears as an integral player in this cooperative, dynamic interplay that ultimately leads to the β-arrestin activation and signaling patterns.

Methods

Initial structures

The initial conformation of β-arrestin 1 was modeled from its inactive structure available in the PDB (PDB: 1G4M)[48]. Modeller v9.19[49] was used to fill missing residues of that protein, selecting the model displaying the lowest DOPE score value for the following simulations.

As no structure is yet solved for the GHSR:β-arrestin 1 complex, initial models were generated by fitting the GHSR active conformation (PDB: 7F9Y[50]) onto the B1AR or the NTS-1 receptor complexed to β-arrestin (PDBs: 6TKO[16] and 6PWC[17]). Doing so, no initial steric clash was observed. The ghrelin peptide was removed from the resulting complexes before running the simulations.

AA simulations

All-atom MD (AAMD) simulations were performed with Gromacs 2020.4[51] on either isolated β-arrestin 1 in water or on the GHSR:β-arrestin 1 complex inserted in a lipid bilayer. AAMD simulations were all carried out using the CHARMM36m force field[52], using TIP3P water molecules and adding Na^+ and Cl^- ions to reach a salt concentration of 0.15 M. The different systems were set up with tools available in CHARMM-GUI[53]. Their energy was first minimized through 500,000 steps of the steepest descent algorithm using a convergence criterion of 1000 kJ $mol^{-1}.nm^{-1}$ and a switching function handling van der Waals forces in the 10-12 Å range. Energy minimization was followed by successive equilibration phases in the NVT ensemble each lasting 25 ps, using an integration step of 1 fs and a Nosé-Hoover thermostat[54,55] to maintain the temperature at 300 K. Several replicas were run using different seeds therefore assuming a random assignment of initial velocities. Long-range electrostatic interactions were computed using the Particle Mesh Ewald (PME) algorithm. During the minimization and the equilibration processes, protein atoms were restrained in position with force constants of 400.0 kJ mol^{-1} nm^{-1} and 40.0 kJ.mol^{-1} nm^{-1}, respectively applied to backbone and side-chains heavy atoms. The subsequent production runs were performed in the NPT ensemble with an integration step of 2 fs, maintaining pressure to 1 bar through a Parrinello-Rahman barostat[56]. For the different systems, the resulting MD trajectories from the production runs were all concatenated and analyzed as a whole.

CGMD simulations

Molecular Dynamics simulations at the Coarse-Grained (CGMD) level were performed using Gromacs[51] version 2020.4 and the MARTINI 3 force field[35]. β-arrestin 1 and the GHSR:β-arrestin 1 complexes were first converted to MARTINI 3 including an elastic network with a 9 Å cutoff using the martinize2 script. The membrane part was generated using the insane script provided by MARTINI tools[57]. The membrane composition was set to 48% of POPC, 32% of POPG, and 20% of cholesterol in each lipid layer to fit that used in the experiments. To study the effect of PI(4,5)P2, a second membrane was built in which 10 POPC were replaced by 10 PI(4,5)P2 molecules in each leaflet. Parameters for PI(4,5)P2 were kindly provided by the group of Paulo Telles de Souza. Isolated β-arrestin 1 was placed at an initial distance above 20 Å from the membrane surface to prevent any initial bias whereas the initial orientation to the membrane of the GHSR:β-arrestin 1 complex was chosen according to the OPM method[58]. After solvation, the global charges of the different systems were neutralized by adding Na^+ and Cl^- ions to reach a salt concentration of 0.15 M. Energy minimization and equilibration steps were done according to the CHARMM-GUI protocol. During equilibration, the positional restraints applied to proteins (backbone atoms) or lipids (heads) were progressively released whereas the integration step was increased from 2 to 20 fs. Initial velocities were randomly generated following a Maxwell–Boltzmann distribution at 300 K, maintaining the temperature using the V-Rescale thermostat[59]. A semi-isotropic pressure coupling was applied maintaining the pressure at 1 bar using the Berendsen barostat[60]. Production runs were performed using the Parrinello-Rahman barostat[56] and all stopped after reaching 30 μs.

Metadynamics

Well-tempered metadynamics[61,62] simulations were performed at the CG level using PLUMED[63] (version 2.8), employing the same parameters as those used in unbiased MD and a bias factor value of 10. The chosen collective variable was the $F71^{1.60}$-L191 distance measured experimentally with no wall applied so that the whole phase space was accessible during the simulations. Gaussians of 0.2 nm width and 0.2 kJ.mol^{-1} height were deposited every 5000 steps (100 ps). These parameters allowed us to sample the expected range of distances in μs time-scale simulations. Simulations were stopped after ~15 μs.

Protein–membrane contact analysis

Protein residues (β-arrestin 1 or GHSR) and membrane lipids were considered in contact when the distance between the respective protein bead and the closest phosphate bead was smaller than 5 Å. To monitor the interaction of the unbiased β-arrestin 1 with the

membrane (Fig. 2C), we calculated the percentage of frames where any bead of the full protein (residues 2–357), the finger loop (residues 64-74), or the C-edge loop (residues 329-339) were in contact with a phosphate bead. To calculate the percentage of trajectory frames where PI(4,5)P2 is in contact with the GHSR:β-arrestin 1 complex, all PI(4,5)P2 beads were considered.

Calculation of β-arrestin 1 "tilt" and "roll" angles

To determine the orientation of β-arrestin 1 at the cell membrane, we calculated "tilt" and "roll" angles by defining the center of mass of backbone (BB) beads of three regions in β-arrestin 1: a) residues 144, 145, and 146 (N-domain); b) residues 323, 324, and 325 (C-domain); and c) residues 56, 57, 58, 80, 81, and 82 (N-domain). We then defined vector 1 (v1) from a to c and vector 2 (v2) from a to b. We generated a new vector called v2o in the same direction as v2, being orthogonal to v1. To obtain "tilt", we calculated the angle between v2o and the Z-axis, perpendicular to the membrane. The final "tilt" angles were calculated by subtracting "tilt" from 90°, thus obtaining angles starting from the membrane plane towards the Z-axis. For "roll", we defined the membrane plane as the XY-axis and calculated the angle of v1 to the plane. "Tilt" goes from 0 to 90° while "roll" goes from o to 180°. Positive or negative angles were determined by the directions of v1 and v2o above or below the membrane plane. For a detailed description, please refer to the supplementary material (Supplementary Fig. 12).

Receptor preparation

Human GHSR and its mutants were expressed in *Escherichia coli* inclusion bodies, folded in amphipol A8-35 from an SDS-unfolded state and then A8-35 was exchanged to n-Dodecyl-β-D-Maltopyranoside (β-DDM) as described[24]. For reconstitution into nanodiscs, the His-tagged receptor in a 50 mM Tris-HCl pH 8, 100 mM NaCl, 2 mM β-DDM was first batch-bound onto a pre-equilibrated Ni-NTA superflow resin. The slurry was then mixed with 10 μM of JMV3011, MSP1E3D1(-) and a POPC:POPG (3:2 molar ratio) mixture containing or not 2.5% PI(4,5)P2 molar ratio at a 0.1:1:75 receptor:MSP:lipid ratio, with the receptor still immobilized on the Ni-NTA matrix. After 1 h incubation at 4 °C, polystyrene beads (Bio-Beads SM-2) were added at an 80% (w/v) ratio and incubated under smooth stirring for 4 h at 4 °C. The resin was then extensively washed with a 50 mM Tris-HCl pH 8, 150 mM NaCl, 1 μM JMV3011 buffer and the His-tagged receptor eluted with the same buffer containing 200 mM imidazole. After extensive dialysis in a 25 mM HEPES, 150 mM NaCl, 0.5 mM EDTA, pH 7.4 buffer, active receptor fractions were purified using affinity chromatography with the biotinylated JMV2959 and homogeneous fractions of GHSR-containing discs finally obtained through a size-exclusion chromatography step on a S200 increase column (10/300 GL) using a 25 mM HEPES, 150 mM NaCl, 0.5 mM EDTA, pH 7.4 buffer as the eluent. For LRET measurement, a truncated receptor where a sortase ligation consensus sequence (LPERGGH) replaced the 346-366 region was produced using the protocol described above. The receptor in nanodiscs was then incubated overnight at 4 °C with 2 μM sortaseA and the peptide GGG-GHSRp where the potential phosphorylation sites in the 346-366 region of GHSR (S349, T350, S362, S363 and T366[41]) had been replaced by their phosphorylated counterpart, as described in ref. 64. Non-ligated receptor was then removed using a HisTrap 1 mL column (Cytiva).

β-arrestin 1 preparation

The full-length cysteine-free β-arrestin 1 mutant and its pre-activated ΔC version with reactive cysteines at positions 68, 167 or 191 were produced as recently described[23]. Briefly, the initial construct was human β-arrestin 1 where all cysteine residues were removed by site-directed mutagenesis (C59V, C125S, C140L, C150V, C242V, C251V, C269S). ΔC β-arrestin 1 was prepared from this construct by truncating the protein at residue 382. Both constructs were then modified by introducing a cysteine at position 68, 167 or 191 by site-directed mutagenesis, and adding an N-terminal hexahistidine tag followed by a 3 C protease site. The sequence was codon-optimized for expression in *E. coli* and cloned into a pET-15b vector (Genecust). NiCo21(DE3) competent *E. coli* (NEB) cells were transformed with the resulting expression vector. Cultures were grown in 2YT medium supplemented with 100 μg/mL carbenicillin at 37 °C up to an OD600 of 1.0. The temperature of the culture was then decreased to 16 °C and protein expression induced with 25 μM IPTG for 20 h. Cells were harvested, resuspended in 50 mM Tris-HCl pH 8, 300 mM NaCl, 15% glycerol, 1 mM TCEP supplemented with a protease inhibitor cocktail (Roche), lysed by sonication, and centrifuged at 27,000xg for 45 min. The supernatant was applied to a HisTrap 5 mL column (Cytiva) and washed with a 50 mM Tris-HCl pH 8, 300 mM NaCl, 15% glycerol, 1 mM TCEP buffer containing 20 mM and then 40 mM imidazole. The protein was eluted with the same buffer containing 200 mM imidazole, dialyzed into a 25 mM Na-HEPES, 200 mM NaCl, 1 mM TCEP, 10% glycerol, pH 7.5 buffer, digested with 3 C protease (16 h at 20 °C) and subjected to reverse-nickel purification. The resulting protein was then diluted with a buffer devoid of NaCl to reach a final NaCl concentration of 40 mM, loaded on a HiSure Q 5 mL column (Cytiva), and eluted with a linear 40 to 400 mM NaCl gradient in 25 mM Na-HEPES, 1 mM TCEP, 10% glycerol, pH 7.5. The protein recovered was then subjected to size-exclusion chromatography using a Superdex 200 increase 10/300 GL column (Cytiva) in a buffer 20 mM HEPES pH7.5, 200 mM NaCl, 10% glycerol, 1 mM TCEP.

Protein labeling

For labeling β-arrestin 1 with MB (ThermoFisher), the latter was added from a 100 mM stock solution in DMSO to purified β-arrestin 1 at a 1:10 molar ratio and incubated overnight at 4 °C in the dark. The reaction was then stopped with 5 mM L-cysteine and unreacted fluorophore removed on a Zeba Spin column (ThermoFisher). Labeling with the Tb-cryptate for the LRET experiments was carried out by incubating the β-arrestin 1 with 2 equivalents of Lumi-4 Tb maleimide (CisBio) overnight at 4 °C, on the one hand, and incubating the GHSR containing a single reactive cysteine at position $71^{1.60}$[39] with Alexa Fluor 488 maleimide (ThermoFisher) at a 1:1.5 receptor-to-dye molar ratio, at 4 °C for 12 h, on the other hand. The protein samples were then desalted on a Zeba Spin column (ThermoFisher). In all cases, the labeling ratios were calculated from the absorption spectra of the labeled proteins using the known extinction coefficients of the receptor and the fluorophores.

MB fluorescence measurements

Empty or GHSR-containing nanodiscs (20 μM) were mixed with purified β-arrestin 1 (2 μM) in a 25 mM HEPES, 50 mM NaCl, pH 7.4 buffer. After incubation for 2 h at 20 °C, fluorescence was measured on a Cary Eclipse spectrometer (Varian) thermostated at 20 °C. For each scan, λexc was set at 380 nm, the excitation and emission bandpass set at 5 nm, and emission measured between 410 nm and 520 nm. Fluorescence intensity was corrected for any dilution effect. For the MB experiments with the probe attached to C191 in β-arrestin 1 and for empty nanodiscs, 10% 16:0 Tempo PC (Avanti polar lipids) were inserted into the nanodiscs[65]. Emission intensity was quantified using the maximum fluorescence emission value. An analysis using the area under the spectrum provided similar outputs (see Supplementary Fig. 13).

LRET measurements

GHSR-containing nanodiscs (20 μM) were mixed with purified β-arrestin 1 (2 μM) in a 25 mM HEPES, 50 mM NaCl, pH 7.4 buffer. After incubation for 2 h at 20 °C, LRET was measured with a spectrometer with a pulsed Xe lamp as the excitation source (λexc: 337 nm, λem: 515 nm; 5 μs steps; 100 μs delay for Alexa Fluor 488 λexc: 337 nm, λem: 544 nm; 5 μs steps; 100 μs delay for BodipyTMR). Donor Tb3 + -chelate

fluorescence decays were recorded for each probe position in donor-only labeled complexes. Three independent measurements were carried out and the mean sensitized emissions were fitted to a multi exponential decay function with DecayFit (FluorTools, www.fluortools.com). The goodness of the exponential fit was determined from the random residual. Lifetime distributions shorter than 100 µs were discarded as these are largely a function of the instrument response time[66]. The components reported in Supplementary Table S1 correspond to the two major time constants of donor fluorescence decay inferred from these exponential fits. The distances between donor and acceptor molecules were estimated from the efficiency of energy transfer[39]. Corresponding populations were estimated from the pre-exponential factors and the excited state lifetime values[42].

Reporting summary

Further information on research design is available in the Nature Portfolio Reporting Summary linked to this article.

Data availability

All the simulation data generated in this study have been deposited in the Zenodo database under accession code 14845654 [https://doi.org/10.5281/zenodo.14845653]. These include (i) gromacs.tpr and PLUMED input files to reproduce both unbiased and biased MD simulations, (ii) processed MD trajectories, and (iii) the different scripts used for analyses. A source data file was also provided with this paper for all experiments. Source data are provided with this paper.

References

1. Hauser, A. S., Attwood, M. M., Rask-Andersen, M., Schiöth, H. B. & Gloriam, D. E. Trends in GPCR drug discovery: new agents, targets and indications. *Nat. Rev. Drug Discov.* **16**, 829–842 (2017).
2. Cheng, L. et al. Structure, function and drug discovery of GPCR signaling. *Mol. Biomed.* **4**, 46 (2023).
3. Jean-Charles, P.-Y., Kaur, S. & Shenoy, S. K. GPCR signaling via β-arrestin-dependent mechanisms. *J. Cardiovasc. Pharmacol.* **70**, 142–158 (2017).
4. Wess, J., Oteng, A.-B., Rivera-Gonzalez, O., Gurevich, E. V. & Gurevich, V. V. β-Arrestins: structure, function, physiology, and pharmacological perspectives. *Pharmacol. Rev.* **75**, 854–884 (2023).
5. Peterson, Y. K. & Luttrell, L. M. The diverse roles of arrestin scaffolds in G protein-coupled receptor signaling. *Pharmacol. Rev.* **69**, 256–297 (2017).
6. He, Q.-T. et al. Structural studies of phosphorylation-dependent interactions between the V2R receptor and arrestin-2. *Nat. Commun.* **12**, 2396 (2021).
7. Min, K. et al. Crystal structure of β-arrestin 2 in complex with CXCR7 phosphopeptide. *Structure* **28**, 1014–1023.e4 (2020).
8. Nobles, K. N. et al. Distinct phosphorylation sites on the β(2)-adrenergic receptor establish a barcode that encodes differential functions of β-arrestin. *Sci. Signal.* **4**, ra51 (2011).
9. Lally, C. C. M., Bauer, B., Selent, J. & Sommer, M. E. C-edge loops of arrestin function as a membrane anchor. *Nat. Commun.* **8**, 14258 (2017).
10. Huang, W. et al. Structure of the neurotensin receptor 1 in complex with β-arrestin 1. *Nature* **579**, 303–308 (2020).
11. Milano, S. K., Kim, Y.-M., Stefano, F. P., Benovic, J. L. & Brenner, C. Nonvisual arrestin oligomerization and cellular localization are regulated by inositol hexakisphosphate binding. *J. Biol. Chem.* **281**, 9812–9823 (2006).
12. Sander, C. L. et al. Structural evidence for visual arrestin priming via complexation of phosphoinositols. *Structure* **30**, 263–277.e5 (2022).
13. Kang, Y. et al. Crystal structure of rhodopsin bound to arrestin by femtosecond X-ray laser. *Nature* **523**, 561–567 (2015).
14. Zhou, X. E. et al. X-ray laser diffraction for structure determination of the rhodopsin-arrestin complex. *Sci. Data* **3**, 160021 (2016).
15. Zhou, X. E. et al. Identification of phosphorylation codes for arrestin recruitment by G protein-coupled receptors. *Cell* **170**, 457–469.e13 (2017).
16. Lee, Y. et al. Molecular basis of β-arrestin coupling to formoterol-bound β 1-adrenoceptor. *Nature* **583**, 862–866 (2020).
17. Yin, W. et al. A complex structure of arrestin-2 bound to a G protein-coupled receptor. *Cell Res.* **29**, 971–983 (2019).
18. Staus, D. P. et al. Structure of the M2 muscarinic receptor–β-arrestin complex in a lipid nanodisc. *Nature* **579**, 297–302 (2020).
19. Bous, J. et al. Structure of the vasopressin hormone–V2 receptor–β-arrestin1 ternary complex. *Sci. Adv.* **8**, eabo7761 (2022).
20. Cao, C. et al. Signaling snapshots of a serotonin receptor activated by the prototypical psychedelic LSD. *Neuron* **110**, 3154–3167.e7 (2022).
21. Liao, Y.-Y. et al. Snapshot of the cannabinoid receptor 1-arrestin complex unravels the biased signaling mechanism. *Cell* **186**, 5784–5797.e17 (2023).
22. Chen, K. et al. Tail engagement of arrestin at the glucagon receptor. *Nature* **620**, 904–910 (2023).
23. Guillien, M. et al. Phosphorylation motif dictates GPCR C-terminal domain conformation and arrestin interaction. *Structure* **31**, 1394–1406.e7 (2023).
24. Damian, M. et al. High constitutive activity is an intrinsic feature of ghrelin receptor protein. *J. Biol. Chem.* **287**, 3630–3641 (2012).
25. Gross, J. D., Zhou, Y., Barak, L. S. & Caron, M. G. Ghrelin receptor signaling in health and disease: a biased view. *Trends Endocrinol. Metab. TEM* **34**, 106–118 (2023).
26. Sommer, M. E., Smith, W. C. & Farrens, D. L. Dynamics of arrestin-rhodopsin interactions: arrestin and retinal release are directly linked events. *J. Biol. Chem.* **280**, 6861–6871 (2005).
27. Kumari, P. et al. Functional competence of a partially engaged GPCR–β-arrestin complex. *Nat. Commun.* **7**, 13416 (2016).
28. Kumari, P. et al. Core engagement with β-arrestin is dispensable for agonist-induced vasopressin receptor endocytosis and ERK activation. *Mol. Biol. Cell* **28**, 1003–1010 (2017).
29. Zhai, R. et al. Distinct activation mechanisms of β-arrestin-1 revealed by 19F NMR spectroscopy. *Nat. Commun.* **14**, 7865 (2023).
30. Damian, M. et al. Allosteric modulation of ghrelin receptor signaling by lipids. *Nat. Commun.* **12**, 3938 (2021).
31. Grimes, J. et al. Plasma membrane preassociation drives β-arrestin coupling to receptors and activation. *Cell* **186**, 2238–2255.e20 (2023).
32. Kovoor, A., Celver, J., Abdryashitov, R. I., Chavkin, C. & Gurevich, V. V. Targeted construction of phosphorylation-independent beta-arrestin mutants with constitutive activity in cells. *J. Biol. Chem.* **274**, 6831–6834 (1999).
33. Kim, K. & Chung, K. Y. Molecular mechanism of β-arrestin-2 pre-activation by phosphatidylinositol 4,5-bisphosphate. *EMBO Rep.* **25**, 4190–4205 (2024).
34. Janetzko, J. et al. Membrane phosphoinositides regulate GPCR-β-arrestin complex assembly and dynamics. *Cell* **185**, 4560–4573.e19 (2022).
35. Souza, P. C. T. et al. Martini 3: a general purpose force field for coarse-grained molecular dynamics. *Nat. Methods* **18**, 382–388 (2021).
36. Sarcinella, M. C. et al. Lipid curvature and fluidity influence lipid incorporation disparities in nanodiscs. *Anal. Chem.* **97**, 2883–2889 (2025).
37. Chen, Q. et al. Structural basis of arrestin-3 activation and signaling. *Nat. Commun.* **8**, 1427 (2017).
38. Mansoor, S. E. & Farrens, D. L. High-throughput protein structural analysis using site-directed fluorescence labeling and the bimane

derivative (2-Pyridyl)dithiobimane. *Biochemistry* **43**, 9426–9438 (2004).
39. Damian, M. et al. Ghrelin receptor conformational dynamics regulate the transition from a preassembled to an active receptor:Gq complex. *Proc. Natl Acad. Sci. USA* **112**, 1601–1606 (2015).
40. Selvin, P. R. Principles and biophysical applications of lanthanide-based probes. *Annu. Rev. Biophys. Biomol. Struct.* **31**, 275–302 (2002).
41. Bouzo-Lorenzo, M. et al. Distinct phosphorylation sites on the ghrelin receptor, GHSR1a, establish a code that determines the functions of ß-arrestins. *Sci. Rep.* **6**, 22495 (2016).
42. Heyduk, T. & Heyduk, E. Luminescence energy transfer with lanthanide chelates: interpretation of sensitized acceptor decay amplitudes. *Anal. Biochem.* **289**, 60–67 (2001).
43. Pacheco, J. et al. Fast-diffusing receptor collisions with slow-diffusing peptide ligand assemble the ternary parathyroid hormone–GPCR–arrestin complex. *Nat. Commun.* **15**, 10499 (2024).
44. Sommer, M. E., Hofmann, K. P. & Heck, M. Distinct loops in arrestin differentially regulate ligand binding within the GPCR opsin. *Nat. Commun.* **3**, 995 (2012).
45. Srivastava, A., Baidya, M., Dwivedi-Agnihotri, H. & Shukla, A. K. Chapter Fourteen - Site-directed labeling of β-arrestin with monobromobimane for measuring their interaction with G protein-coupled receptors. In *Methods in Enzymology* (ed. Shukla, A. K.) vol. 633 271–280 (Academic Press, 2020).
46. Aydin, Y. et al. Structural details of a Class B GPCR-arrestin complex revealed by genetically encoded crosslinkers in living cells. *Nat. Commun.* **14**, 1151 (2023).
47. Mayer, D. et al. Distinct G protein-coupled receptor phosphorylation motifs modulate arrestin affinity and activation and global conformation. *Nat. Commun.* **10**, 1261 (2019).
48. Han, M., Gurevich, V. V., Vishnivetskiy, S. A., Sigler, P. B. & Schubert, C. Crystal structure of β-arrestin at 1.9 Å: possible mechanism of receptor binding and membrane translocation. *Structure* **9**, 869–880 (2001).
49. Webb, B. & Sali, A. Comparative protein structure modeling using MODELLER. *Curr. Protoc. Bioinform.* **54**, 5.6.1–5.6.37 (2016).
50. Wang, Y. et al. Molecular recognition of an acyl-peptide hormone and activation of ghrelin receptor. *Nat. Commun.* **12**, 5064 (2021).
51. Abraham, M. J. et al. GROMACS: High performance molecular simulations through multi-level parallelism from laptops to supercomputers. *SoftwareX* **1–2**, 19–25 (2015).
52. Huang, J. et al. CHARMM36m: an improved force field for folded and intrinsically disordered proteins. *Nat. Methods* **14**, 71–73 (2017).
53. Lee, J. et al. CHARMM-GUI input generator for NAMD, GROMACS, AMBER, OpenMM, and CHARMM/OpenMM simulations using the CHARMM36 additive force field. *J. Chem. Theory Comput.* **12**, 405–413 (2016).
54. Nosé, S. A unified formulation of the constant temperature molecular dynamics methods. *J. Chem. Phys.* **81**, 511–519 (1984).
55. Hoover, W. G. Canonical dynamics: equilibrium phase-space distributions. *Phys. Rev. A* **31**, 1695–1697 (1985).
56. Parrinello, M. & Rahman, A. Polymorphic transitions in single crystals: a new molecular dynamics method. *J. Appl. Phys.* **52**, 7182–7190 (1981).
57. Wassenaar, T. A., Ingólfsson, H. I., Böckmann, R. A., Tieleman, D. P. & Marrink, S. J. Computational lipidomics with insane: a versatile tool for generating custom membranes for molecular simulations. *J. Chem. Theory Comput.* **11**, 2144–2155 (2015).
58. Lomize, M. A., Pogozheva, I. D., Joo, H., Mosberg, H. I. & Lomize, A. L. OPM database and PPM web server: resources for positioning of proteins in membranes. *Nucleic Acids Res.* **40**, D370–376 (2012).
59. Bussi, G., Donadio, D. & Parrinello, M. Canonical sampling through velocity rescaling. *J. Chem. Phys.* **126**, 014101 (2007).
60. Berendsen, H. J. C., Postma, J. P. M., van Gunsteren, W. F., DiNola, A. & Haak, J. R. Molecular dynamics with coupling to an external bath. *J. Chem. Phys.* **81**, 3684–3690 (1984).
61. Barducci, A., Bussi, G. & Parrinello, M. Well-tempered metadynamics: a smoothly converging and tunable free-energy method. *Phys. Rev. Lett.* **100**, 020603 (2008).
62. Laio, A. & Parrinello, M. Escaping free-energy minima. *Proc. Natl Acad. Sci. USA* **99**, 12562–12566 (2002).
63. Bussi, G. & Tribello, G. A. Analyzing and biasing simulations with PLUMED. *Methods Mol. Biol. Clifton NJ* **2022**, 529–578 (2019).
64. Staus, D. P. et al. Sortase ligation enables homogeneous GPCR phosphorylation to reveal diversity in β-arrestin coupling. *Proc. Natl Acad. Sci. USA* **115**, 3834–3839 (2018).
65. Wang, Y. et al. Identification of shallow and deep membrane-penetrating forms of diphtheria toxin T domain that are regulated by protein concentration and bilayer width. *J. Biol. Chem.* **272**, 25091–25098 (1997).
66. Zoghbi, M. E. & Altenberg, G. A. Luminescence resonance energy transfer spectroscopy of ATP-binding cassette proteins. *Biochim. Biophys. Acta Biomembr.* **1860**, 854–867 (2018).

Acknowledgements

We thank CNRS, Université de Montpellier, Agence Nationale de la Recherche (ANR-20-CE92-0028, ANR-21-CE29-0012, ANR-22-CE44-0042), and the Fondation Pour la Recherche Médicale (FRM, Equipe FRM EQU202103012736) for their financial support. This work was granted access to the HPC resources of IDRIS and CINES under the allocations A0100712444, A0140714133 and A0160715115 made by GENCI. We thank Dr. Paulo Cesar Telles de Souza for helpful discussions on using the MARTINI 3 force field and to have provided us with PI(4,5)P2 parameters. We are also grateful to the program CAPES-COFECUB (project Ph-C 882-17) which promoted the collaboration between the French and Brazilian teams.

Author contributions

A.A.S.G., M.D.M., M.L., J.L.B., and N.F. designed the research. A.A.S.G., R.A.R., M.L., and N.F. performed and analyzed MD simulations. M.D.M., M.D., and J.L.B. performed experiments and analyzed the corresponding data. N.F. and J.L.B. wrote the original draft. A.A.S.G., M.D.M., R.A.R., P.M.B., N.S., M.L., J.L.B., and N.F. reviewed and edited the paper. All authors contributed to the interpretation of the data, and read and approved the final manuscript.

Competing interests

The authors declare no competing interests.

Additional information

Supplementary information The online version contains supplementary material available at https://doi.org/10.1038/s41467-025-59842-8.

Correspondence and requests for materials should be addressed to Nicolas Floquet.

Peer review information *Nature Communications* thanks Irina Kufareva and the other, anonymous, reviewer(s) for their contribution to the peer review of this work. A peer review file is available.